Induced polarized state in intentionally grown oxygen deficient $KTaO_3$ thin films

D. A. Mota, Y. Romaguera-Barcelay, A. Tkach' , J. Pérez de la Cruz, P. M. Vilarinho, P. B. Tavares, J. Agostinho Moreira, and A. Almeida'

Citation: Journal of Applied Physics **114**, 034101 (2013); doi: 10.1063/1.4813324
View online: http://dx.doi.org/10.1063/1.4813324
View Table of Contents: http://aip.scitation.org/toc/jap/114/3
Published by the American Institute of Physics

Induced polarized state in intentionally grown oxygen deficient $KTaO_3$ thin films

D. A. Mota,[1] Y. Romaguera-Barcelay,[1] A. Tkach,[1,a)] J. Pérez de la Cruz,[2] P. M. Vilarinho,[3] P. B. Tavares,[4] J. Agostinho Moreira,[1] and A. Almeida[1,b)]
[1]*IFIMUP and IN Institute of Nanoscience and Nanotechnology, Department of Physics and Astronomy, Faculty of Science of University of Porto, Rua do Campo Alegre, 687, 4169 007 Porto, Portugal*
[2]*INESC TEC, Rua do Campo Alegre, 687, 4169 007 Porto, Portugal*
[3]*Department of Ceramics and Glass Engineering, CICECO, University of Aveiro, 3810 193 Aveiro, Portugal*
[4]*Centro de Química, Universidade de Trás os Montes e Alto Douro, Apartado 1013, 5001 801 Vila Real, Portugal*

(Received 15 May 2013; accepted 17 June 2013; published online 15 July 2013)

Deliberately oxygen deficient potassium tantalate thin films were grown by RF magnetron sputtering on $Si/SiO_2/Ti/Pt$ substrates. Once they were structurally characterized, the effect of oxygen vacancies on their electric properties was addressed by measuring leakage currents, dielectric constant, electric polarization, and thermally stimulated depolarization currents. By using K_2O rich $KTaO_3$ targets and specific deposition conditions, $KTaO_{3-\delta}$ oxygen deficient thin films with a $K/Ta = 1$ ratio were obtained. Room temperature X-ray diffraction patterns show that $KTaO_{3-\delta}$ thin films are under a compressive strain of 2.3% relative to $KTaO_3$ crystals. Leakage current results reveal the presence of a conductive mechanism, following the Poole-Frenkel formalism. Furthermore, dielectric, polarization, and depolarization current measurements yield the existence of a polarized state below $T_{pol} \sim 367\,^{\circ}C$. A Cole-Cole dipolar relaxation was also ascertained apparently due to oxygen vacancies induced dipoles. After thermal annealing the films in an oxygen atmosphere at a temperature above T_{pol}, the aforementioned polarized state is suppressed, associated with a drastic oxygen vacancies reduction emerging from annealing process.
 [http://dx.doi.org/10.1063/1.4813324]

I. INTRODUCTION

Among materials with high dielectric constant, perovskite compounds such as $SrTiO_3$, $KTaO_3$, or $CaTiO_3$ that do not exhibit any ferroelectric (FE) phase transition but continuous increase of the dielectric constant with temperature decreasing down to 0 K (Ref. 1) can be found. These materials are classified as incipient ferroelectrics and possess a highly polarizable lattice. Consequently, their properties are very sensitive to impurities, strain, and applied electric fields. These factors can induce ferroelectricity, intermediate-glass, or relaxor-like states, turning such systems very attractive from both fundamental and technological point of view.

$KTaO_3$ shows at room temperature the same crystal structure (cubic, $Pm3m$ space group) as $SrTiO_3$.[2] The temperature behavior of the static dielectric constant can be understood by considering the low temperature softening of the TO_1 ferroelectric soft mode into the Lyddanne-Sachs-Teller relation.[3–5] The static dielectric constant reaches up to 5000 below 10 K, whilst $KTaO_3$ keeps its perovskite cubic symmetry.[5] Electric field, doping,[3,6] and strain[7] may change the balance between the ferroelectric ordering and the zero-point quantum fluctuations of Ta^{5+} ions,[8] yielding a lowering of symmetry and allowing for the emergence of a ferroelectric state at finite temperatures. Moreover, the anharmonicity of the TO_1 mode yields the basic conditions for voltage-induced tuning of the dielectric constant, reaching values even larger than those obtained in $SrTiO_3$,[9] while dielectric losses in the microwave range are significantly lower.[10] In this regard, $KTaO_3$ has become a highly interesting matter of research both from fundamental physics and electronic applications.

In order to stabilize the ferroelectric phase at room temperature in $KTaO_3$, it is noteworthy to use crystallographic strain.[7,11–14] Thin films are most attractive, since strain can be tailored through the mismatch of the in-plane lattice parameters of the film material and the substrate. In such conditions, the stabilization of a strain-mediated ferroelectric ground state was predicted from both phenomenological and first-principles models, as it was observed in of $SrTiO_3$-based thin films.[7,12,14,15]

Ferroelectric ground state in $KTaO_3$ thin films on different substrates was reported using different depositions techniques and proved by diverse experimental techniques.[15,16] In Ref. 15, a 10 nm thick epitaxial $KTaO_3$ thin film prepared by pulsed laser deposition on single-crystalline (001) $SrTiO_3$ substrate was studied. The small thickness of the film was chosen in order to avoid significant strain relaxation. In this system, the high-temperature FE phase transition close to $T_m = 760$ K was experimentally proved by the low-frequency dielectric peak with frequency independent T_m, FE-type dielectric nonlinearity, and FE-type temperature variation of optical index of refraction. Contrarily, in Ref. 16, a 200 nm polycrystalline $KTaO_3$ thin film prepared on (0001) sapphire

a)Present address: Institute of Physics, Johannes Gutenberg University Mainz, D 55099, Mainz, Germany.
b)Electronic mail: amalmeid@fc.up.pt

substrate by chemical solution deposition was used. The in-plane complex dielectric spectroscopy obtained from THz time-domain spectroscopic data along with those obtained from dielectric measurements in GHz range evidenced a transition close to 60 K. The experimental results emphasize the contribution for the dielectric constant of the soft mode, which shows a classical softening at ~60 K. Moreover, the existence of a central peak coupled to the soft mode is in favor for the occurrence of a ferroelectric phase in the vicinity of 60 K. It is worth noting that other authors[17] using chemical solution deposition on SiO_2 glass and (100) Si substrates did not obtain in the grown KTO thin films any sign of ferroelectricity, just yielding a hardening of the soft mode which was associated with film porosity and loss of inversion center.

Defect physics is probably one of the most challenging problems that have to be addressed. The presence of defects can alter the macroscopic properties of a material, which will either cause performance degradation or improve it. For example, a very interesting type of defect[18] and at the same time capable to induce a polar state in the $KTaO_3$ system is the introduction of oxygen vacancies which can lead to lattice distortions as reported in other perovskites.[19–21] Oxygen deficiency can be intentionally achieved in different ways, like nonstoichiometric growth, extrinsic doping, or in nonannealed samples.[22] Moreover, in cubic perovskites, the symmetry of electronic states localized near the oxygen vacancy may be spontaneously broken if the electron-lattice interaction overcomes kinetic energy of electron motion.[20] The introduction of oxygen vacancies is particularly important for thick films, where the strain will relax and may not be enough to induce polar properties.

The effect of oxygen deficiency in quantum paraelectrics on their polar and dynamic properties has been studied by several authors. Jandl *et al.*[23] performed a Raman and near-infrared fluorescence analysis of pure and reduced $KTaO_3$ samples and observed stronger infrared luminescence of the Ta^{3+} ions and concluded that the oxygen vacancies are at the origin of the polar microregions. More recently, the same authors reported an infrared study of oxygen vacancies in $KTaO_3$ crystal.[24] They have found that the infrared reflectance is strongly perturbed relative to pure crystals, while Raman spectra are only slightly affected. They interpret the disappearance in the infrared reflectance spectra of the ferroelectric soft mode at all temperatures due to the overdamping by partial disturbances in the Ta-O-Ta chains which reflects the important role played by the oxygen polarizability, the Ta-O-Ta chains, and the long-range interactions. Though an increasing number of works have been published on the effect of oxygen vacancies in quantum paraelectrics, like $KTaO_3$, the study of the electric properties is inexistent and the main mechanisms are far from being completely understood.

This work is thus aimed at studying the physical behavior of intentionally grown $KTaO_{3-\delta}$ thin films deposited on a $Si/SiO_2/Ti/Pt$ substrate by radiofrequency magnetron sputtering. The as-processed films were characterized by carrying out chemical, structural, and microstructural studies. Structural data of the films were used in order to evaluate any lattice distortion, which could be induced in the films by the substrate. Conductive experiments were performed to search for the occurrence of leakage currents and to find out what kind of mechanisms can be involved in, by using appropriate theoretical models. The number of oxygen vacancies plays important role in determining the dielectric properties of the film. An increased number of oxygen vacancies increases the total polarizability by increasing the number of defect dipoles[25,26] and the ionic polarizability. As dipoles can be induced by oxygen vacancies,[25,26] the existence of a polarized state was addressed by performing dielectric and polarization measurements. Such a kind of state actually exists in the as-grown $KTaO_{3-\delta}$ thin films, which can be suppressed by drastically reducing oxygen vacancies.

II. EXPERIMENT

The $KTaO_{3-\delta}$ films were grown on $Si/SiO_2/Ti/Pt$ substrates, using a 2-inch K_2O rich $KTaO_3$ ceramic target. The potassium excess was added to compensate the expected loss of this constituent during deposition. All the depositions were carried out in argon atmosphere, starting for a typical chamber base pressure of 5×10^{-4} Pa. The minimum total purity of the argon used is better than 99.999%. In order to eliminate contaminants and to clean the target surface, a pre-sputtering process was carried out for 10 min at an argon chamber pressure of 1.0 Pa. The substrates were placed in an on-axis position, 5 cm from the target surface plane. During deposition, the substrate temperature was kept constant at 700 °C. After the deposition, the films were cooled down toward room temperature at a rate of approximately 200 °C/h and at the same base pressure used prior to the deposition. These experimental conditions without the use of any external oxygen source ensure the formation of a $KTaO_{3-\delta}$ phase.

To optimize the deposition conditions to yield K/Ta = 1 ratio films, several sets of films were prepared at different argon chamber pressure from 0.5 to 1.2 Pa and RF power from 50 to 100 W, while the other parameters remain constant.

The crystallinity of the films was analyzed using a PAN'alytical X'Pert MPD X-ray diffractometer, equipped with a X'Celerator detector and secondary monochromator, with Cu Kα radiation ($\lambda = 0.15418$ nm). The patterns were recorded in continuous mode in the 2θ range of 20 90°, using a scan step of 0.017° and 100 s/step. The elemental composition of the films was estimated by an energy dispersive X-ray spectroscopy detector attached to a FEI Quanta 400 FEG ESEM scanning electron microscope that was also used to analyze the morphology and measure the thickness of the KTO films.

Gold electrodes were deposited on film surface by sputtering and using suitable masks to perform electric and dielectric measurements. Leakage current measurements on the non-annealed $KTaO_{3-\delta}$ thin films were performed at room temperature using a programmable picoammeter Keithley 6487 controlled by a LABVIEW® program. Dielectric response was measured using an Agilent E4980A LCR meter. The complex dielectric constant $\varepsilon^* = \varepsilon' - j\varepsilon''$ was determined from capacity and dielectric losses provided by the LCR meter, using an a.c. measuring voltage of 50 mV. Thermally stimulated depolarization current was measured

with a standard short circuit method as a function of temperature,[27] while keeping the heating rate constant. Electric polarization (P) versus an a.c. electric field (E) curves were determined using a modified Sawyer-Tower circuit.[28] The electric field was driven at a frequency of 1.3 Hz in order to avoid after-effects associated with polarization reversal. Electrical and dielectric properties were studied in the temperature range of 0 to 400 °C by using a THMS600 Linkam furnace. The temperature was measured with an accuracy of 0.1 °C. In order to simulate the same working conditions used in some electrical measurements and to figure out the real origin of the polar properties, the studied $KTaO_{3-\delta}$ films were annealed at 400 °C during 30 min with an oxygen flux of 0.1 L/min. Towards determining whether the changes in the electric properties of the films come from the electrodes or the annealing process alone, in some of them gold electrodes were only deposited after annealing.

III. RESULTS AND DISCUSSION

A. Chemical, morphological, and structural characterization

The films grown under different deposition parameters were studied by energy dispersive X-ray spectroscopy (EDS). Though it was observed that depending on the deposition parameters used, the as-prepared films presented different K/Ta ratios, in the following just the films with a K/Ta ∼ 1 ratio are considered.

Figure 1 shows the EDS spectrum of a $KTaO_{3-\delta}$ film grown on $Si/SiO_2/Ti/Pt$ under the deposition parameters, which lead to K/Ta ratio close to 1 and undetectable amount of impurities. We verified that a low argon pressure of ∼0.5 Pa, yields $KTaO_{3-\delta}$ thin films with a close K/Ta = 1 ratio. This can be associated with the dissimilar scattering effect of unequal atomic masses (i.e., $M_K = 39.098$ g/mol and $M_{Ta} = 180.948$ g/mol in an argon atmosphere with $M_{Ar} = 39.948$ g/mol) and also with the different components thermalization resulting from the collisions with the argon atoms. Thus, it is expectable that a larger amount of tantalum can be found in the films, due to its large atomic mass and lower scattering effect in an argon atmosphere. The low RF

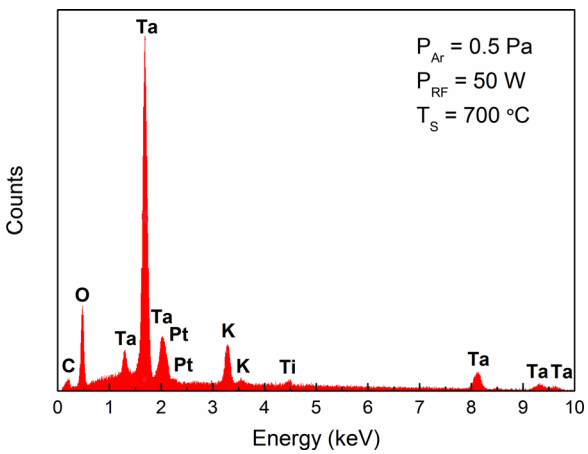

FIG. 1. EDS spectra of $KTaO_{3-\delta}$ thin films deposited at 0.5 Pa and 50 W.

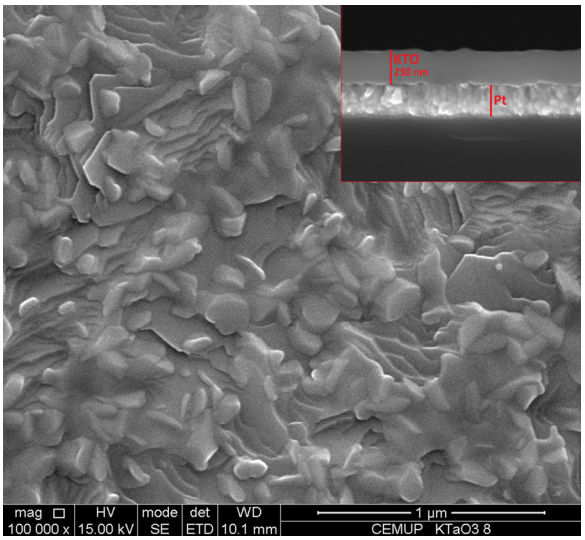

FIG. 2. Plan view SEM image of $KTaO_{3-\delta}$ thin film deposited at 0.5 Pa and 50 W. Inset shows the Pt and KTO layers in cross section SEM image.

power of 50 W yields K/Ta ratio close to one as well, preventing undesirable re-sputtering processes at film surface. This process is even more critical for the case of potassium, as it carries a larger sputtering yield, which can be inferred from its melting point temperature $T_{M,K} = 63.38$ °C.

Figure 2 shows the surface morphology of the $KTaO_{3-\delta}$ films deposited with a RF power of 50 W and in an argon pressure of 0.5 Pa. The growth of the film seems to evolve in a grained, layer-by-layer structural mode that can be associated with either coalescence or coarsening phenomena. The cross-section of the $KTaO_{3-\delta}$ film, shown in the inset of Figure 2, reveals a homogenous uniform structure. From the same inset, it can be also determined that the average thickness of the films is around 230 nm.

Figure 3(a) shows the X-ray diffraction (XRD) pattern of $KTaO_{3-\delta}$ film deposited at an argon pressure of 0.5 Pa and RF power of 50 W. The peaks labeled with (*) are associated with the substrate. The analysis of the XRD pattern reveals that besides small peaks, which will be shown below to be associated with a phase distorted by high concentration of

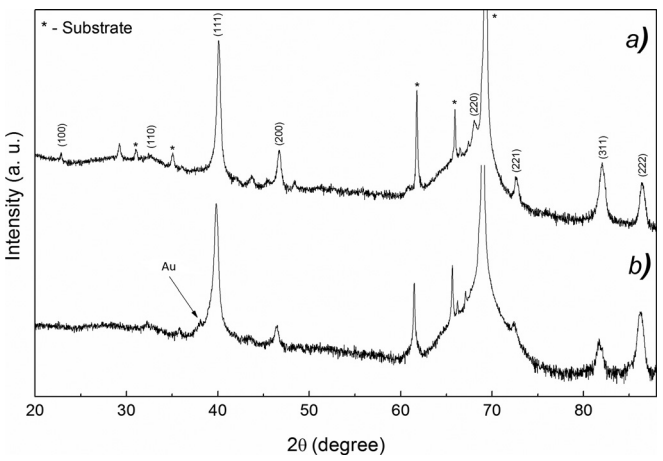

FIG. 3. Room temperature X ray diffraction patterns of as prepared (a) and annealed in oxygen at 400 °C (b) $KTaO_{3-\delta}$ thin film deposited at 0.5 Pa and 50 W.

oxygen vacancies δ, the film apparently crystallize in a cubic symmetry with a P$m3m$ space group, in close agreement with Ref. 29 and shows a preferential growth along the (111) direction. The angular position of the P$m3m$ peaks was obtained by fitting pseudo-Voigt profiles to the experimental results and the lattice parameter of $KTaO_{3-\delta}$ film was determined as $a_{film} = 3.896 \pm 0.001$ Å. By using this value the strain state in the films defined as $s_{film} = (a_{film} \quad a_0)/a_0$, where a_{film} is the lattice parameter of the $KTaO_{3-\delta}$ film and $a_0 = 3.989 \pm 0.001$ Å stands for the lattice parameter of $KTaO_3$ single crystals,[29] was determined. The strain was found to be compressive with a magnitude of approximately 2.3%. It is important to note that the film thickness is about 230 nm, and at this point, the films should be elastically relaxed. However, oxygen vacancies, intentionally incorporated during the deposition procedure, induce lattice distortions on the TaO_6 octahedron[21] and expansion of the unit cell,[30,31] which together with extrinsic stresses associated with lattice mismatch and thermal mismatch between the substrate and thin film material and intrinsic stresses associated with impurities or defects like grain boundaries or dislocations lead to such a deviation between oxygen deficient $KTaO_3$ thin films and single crystals. The thermal mismatch plays an import role in this situation due to the large difference between the coefficient of thermal expansion of the KTO and the platinum. The thermal expansion coefficient of platinum is much larger than that of KTO; thus, cooling the sample after its processing at 700 °C may induce a compressive strain in the film.

The XRD pattern of the annealed $KTaO_{3\ \delta}$ film at 400 °C in an oxygen flux during 30 minutes, shown in Figure 3(b), reveals mainly the P$m3m$ and substrate peaks. The peak marked with an arrow in Figure 3(b) corresponds to metallic gold from electrodes deposited on the film surface. Comparing XRD patterns of the as-prepared and annealed $KTaO_{3-\delta}$ films, small peaks, which could not be indexed in the cubic P$m3m$ symmetry or attributed to the substrate for the as-prepared film, are suppressed by the annealing process. So they have to be ascribed to a phase distorted by high concentration of oxygen vacancies δ. Following the same procedure as described above, the lattice parameter of the annealed film was found to be of 3.920 ± 0.001 Å, indicating the reduction of compressive strain to 1.7%. This strain reduction could be associated with a competition between the reduction of oxygen vacancies concentration in the film which will increase the attractive force among atoms in the film with relief of some internal thermal strains, grain nucleation and defects annihilation. This is provided from the supply of thermal energy and very slow cooling rate of the annealing treatment.

B. Leakage current studies

Figure 4 depicts the leakage current density versus the applied electric field, $J = J(E)$ of non-annealed $KTaO_{3\ \delta}$ thin films at room temperature. $J = J(E)$ curve is slightly asymmetric, which is apparently associated with different work functions of bottom platinum (5.3 eV) and top gold (5.1 eV) electrodes.[32]

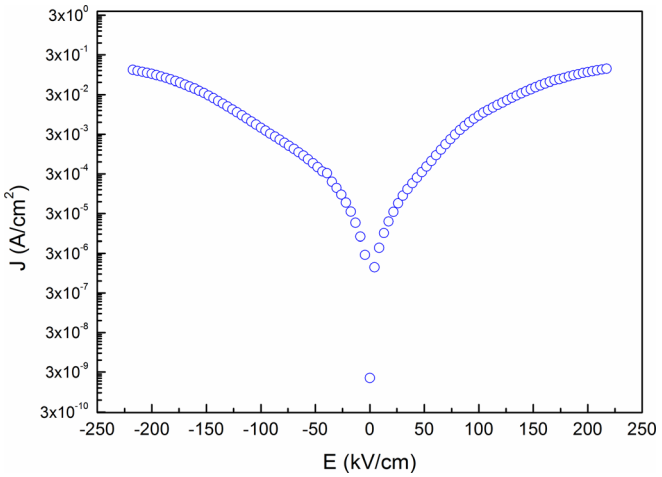

FIG. 4. Leakage current density versus applied electric field for the $KTaO_{3\ \delta}$ thin film.

In order to understand the conduction mechanism in $KTaO_{3\ \delta}$ films several leakage models, such as the Schottky emission (SE), Simmons and Poole-Frenkel (PF) were considered.[33,34] The SE is interface limited and caused by the thermionic injection of carriers from metal electrode into the film. According to SE, the current density is given by

$$J = A^{**}T^2 \exp\left[\frac{-q(\varphi_B - \sqrt{qE/4\pi\varepsilon_0\varepsilon}}{kT}\right], \qquad (1)$$

where J is the current density, A^{**} is the effective Richardson constant, T is the temperature, q is the electronic charge, φ_B is the Schottky barrier height, E is the electric field, ε_0 is the permittivity in vacuum, ε is the optical dielectric constant, and k is the Boltzmann constant.

Although the SE model fits to some of the experimental data as shown in Figure 5, data handling leads to non-physical values of ε ($\varepsilon = 0.19$). The SE model is mainly used when the mobility is high and transport is limited by the recombination velocity at the potential barrier maximum.

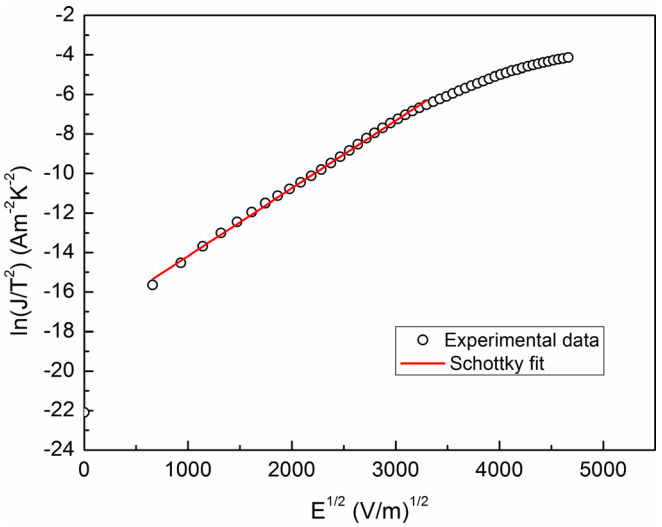

FIG. 5. The Schottky emission plot of $\ln(J/T^2)$ versus $E^{1/2}$ for the $KTaO_{3\ \delta}$ thin film.

In case of reduced mobility, which in our case could be associated with scattering on grain boundaries, a more appropriate model would be the use of the Simmons expression,

$$J = \alpha T^{3/2} E \mu \left(\frac{m^*}{m_0}\right)^{3/2} \exp\left(-\frac{\emptyset_b}{kT}\right) \exp(\beta\sqrt{E}), \qquad (2)$$

which takes into account both the mobility, a bulk property, and the carrier density at the potential barrier maximum near the interface and where $\alpha = 300\,A\,s\,m^{-3}$, μ is the electron mobility, m^* is the effective mass, m_0 is the electron rest mass, $\beta = (e/kT)(4\pi\varepsilon_0\varepsilon)^{1/2}$, $\emptyset_B$ is the barrier height, and e is the electron charge. As it is seen from Figure 6, which shows the plot of $ln(J/E)$ versus $E^{1/2}$ at room temperature, the data can be well fitted with the Simmons equation from 0 to 109 kV/cm. Despite this model yields a reasonable value of the barrier height, $\emptyset_B = 0.445$ eV, a non-physical value for the optical dielectric constant, $\varepsilon = 0.864$, is obtained.

The Poole-Frenkel mechanism is bulk limited and is governed by carriers that are thermally emitted from trapped centers under a strong electric field. According to Poole-Frenkel emission, the current density is expressed as,

$$J = AE\exp(-\emptyset_T/kT)\exp(\beta' E^{1/2}), \qquad (3)$$

where $A = 4\alpha$, $\emptyset_T$ is the trapped level and $\beta' = (e/kT)(4\pi\varepsilon_0\varepsilon)^{1/2}$. The magnitude of the electric field E was calculated by dividing the applied voltage by the thickness of the film, since the Poole-Frenkel emission is mostly a bulk mechanism.

The PF conduction mechanism could be fitted to the experimental data limited to the range from 0 to 109 kV/cm. From this field up to the maximum field, neither the aforementioned models nor the Fowler-Nordheim tunneling model[34] can fit the experimental data, probably due to more complex contribution of several mechanisms to the leakage current.

The validity of this model has been verified by the determination of both optical dielectric constant ε and trapped level $\emptyset_T$ from the plot of $ln(J/E)$ versus $E^{1/2}$ shown in Figure 6. The data were well fitted to the Poole-Frenkel model yielding a trapped level $\emptyset_T = 0.44$ eV, and an optical dielectric constant $\varepsilon = 3.46$, corresponding to a refractive index $n = 1.86$. It is worth noting that the value of $\varepsilon = 3.46$ is similar but slightly smaller than the value referred to in earlier literature for $KTaO_3$ single crystals, which is close to 4.6.[34,35] The results obtained using the Poole-Frenkel formalism are in good agreement with the effect caused by the incorporation of the oxygen vacancies during the growth process of the films.

C. Dielectric studies

The dielectric response of $KTaO_{3-\delta}$ thin films was measured in the frequency range from 20 Hz up to 2 MHz. The capacity (C) and dielectric loss (D) of the film in this frequency range were determined at each fixed temperature in the temperature range of 20 to 400 °C, by sweeping the frequency of the a.c. measuring field over 200 different

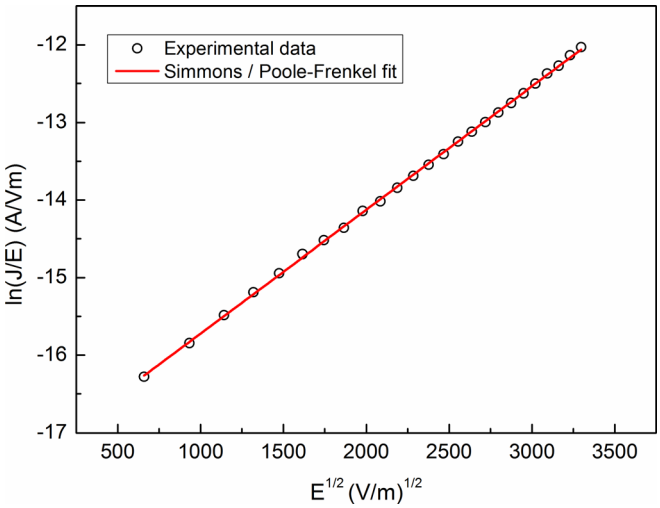

FIG. 6. The Simmons and Poole Frenkel plot of ln(J/E) versus $E^{1/2}$ for the $KTaO_{3-\delta}$ thin film.

frequencies. From the experimental values of the capacity and dielectric losses, and the following equations:

$$\varepsilon(w) = \varepsilon' - j\varepsilon'', \qquad (4)$$

$$\varepsilon' = \frac{Cd}{\varepsilon_0 A}, \qquad (5)$$

$$\varepsilon'' = \varepsilon' D, \qquad (6)$$

the real (ε') and the imaginary (ε'') parts of the dielectric constant can be evaluated, where d is the thickness of the film, A the area of the electrodes, and ε_0 the vacuum permittivity.

Figure 7 shows the relation $\varepsilon'' = \varepsilon''(\varepsilon')$ at three different fixed temperatures, wherein two major outcomes can be highlighted. On one hand, the stretched parts of the curves in the low frequency range can be associated with conducting processes in the film, in good agreement with results obtained in earlier published works.[36] This interpretation will be reinforced by the analysis presented further below. On the second hand, we observe that the most significant contribution to the dielectric constant in the upper range of frequencies is associated with a relaxation process apparently due to reorientation of oxygen vacancies induced dipoles.

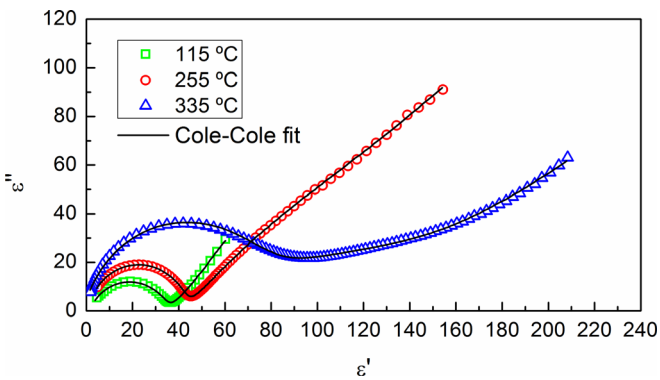

FIG. 7. Complex dielectric constant of the $KTaO_{3-\delta}$ film in the (ε', ε'') plane at temperatures of 115, 255, and 335 °C.

TABLE I. Resistivity and λ for three different fixed temperatures.

T (°C)	ρ (Ω m)	λ
335	2×10^3	0.41
255	6×10^3	0.47
115	9×10^4	0.45

In order to get insight regarding the nature of the relaxation process, the available experimental data were analyzed using a Cole-Cole formalism for the complex dielectric constant, following the equation

$$\varepsilon(\omega) = \varepsilon(\infty) + \frac{\Delta\varepsilon}{1 + (j\omega\tau)^{\beta}} + \frac{1}{(j\omega\tau_c)^{\lambda}}, \quad (7)$$

where $\varepsilon(\infty)$ stands for the high frequency contribution to the dielectric constant. $\Delta\varepsilon$ is the step of the corresponding real part across the Cole-Cole relaxation process, τ is the inverse of the angular relaxation frequency, and β is an exponent ranging from 0 to 1 that reflects the distribution of the relaxation time.[36,37] The value of 1 is characteristic of a mono-dispersive medium. Furthermore, τ_c is the relaxation time associated with conductivity, and λ reflects the dispersion of τ_c.

The solid lines in Figure 7 stand for the best fittings of equation (7) to the experimental data. Table I shows the resistivity (ρ) and λ values obtained from the fitted procedure for the three chosen fixed temperatures in Figure 7. The low values of ρ and λ corroborates the existence of oxygen vacancies in the as-processed films, as also revealed to above by the Poole-Frenkel formalism.

Figure 8 shows the temperature dependence of $\Delta\varepsilon$ and $f_{rel} = 1/\tau$ obtained through the fitting procedure, where it is observed that $\Delta\varepsilon$(T) reveals a defined maximum close to 367 °C. Contrarily, the relaxation frequency shows a broad maximum close to 250 °C. This behavior evidences the existence of a complex relaxation process occurring in the films.[38–40]

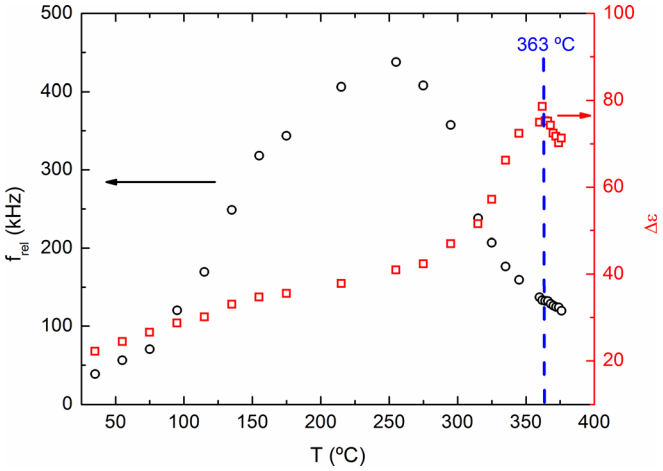

FIG. 8. Temperature dependence of $\Delta\varepsilon$ and f_{rel} fitting parameters for the $KTaO_{3-\delta}$ film.

The value of $\varepsilon(\infty)$ obtained is rather low (~5), which is similar to the one for the optical dielectric constant, obtained from the Poole-Frenkel formalism. This is a surprising result, since it would mean a drastic reduction of the phonon contribution to $\varepsilon(\infty)$. In fact, what we are measuring in the as-prepared films is not the actual lattice contribution to the dielectric constant as it is the case in $KTaO_3$ single crystals, but instead a complex contribution involving non-intrinsic conductive and relaxation phenomena originated by the inclusion of oxygen vacancies in the films.

D. Electrical polarization studies

In order to sort out whether the state below 367 °C, which is marked by the anomaly in $\Delta\varepsilon$(T), is a polarized one, we have studied the temperature dependence of both

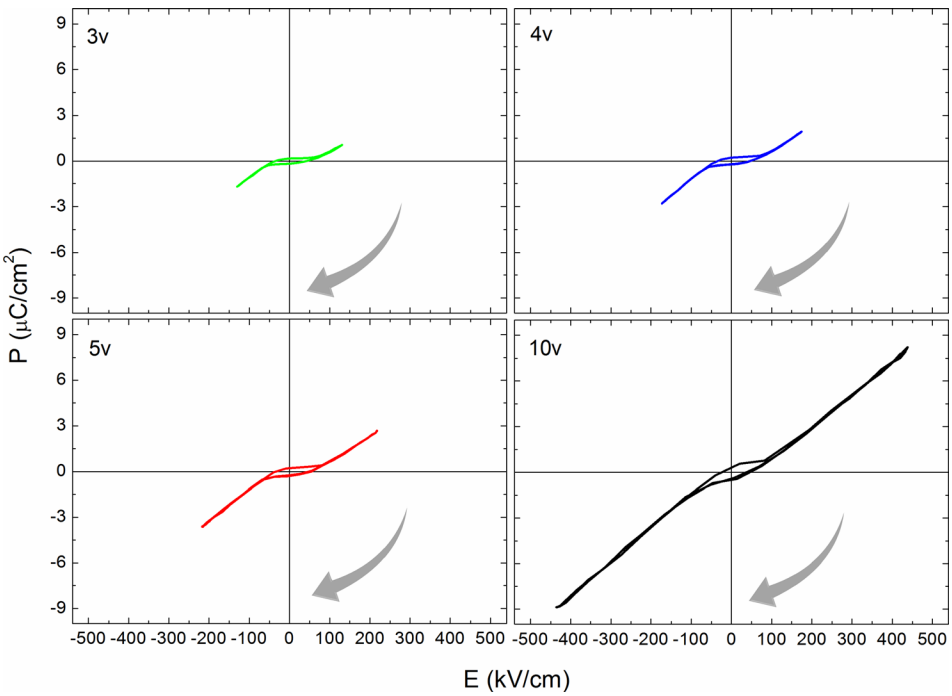

FIG. 9. Room temperature $P(E)$ curves of $KTaO_{3-\delta}$ thin films under maximum applied voltage of 3, 4, 5, and 10 V. The arrows show the direction in which the P $P(E)$ curve is being drawn.

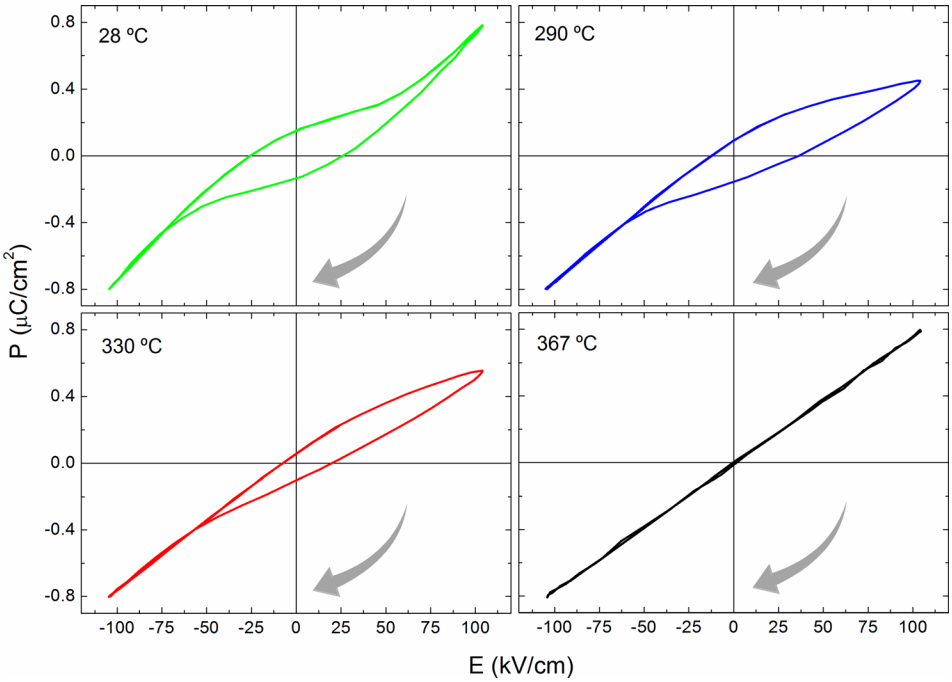

FIG. 10. $P(E)$ curves of $KTaO_{3-\delta}$ thin films at temperatures of 28, 290, 330, and 367 °C.

thermally stimulated depolarization currents and electric polarization (P) versus applied a.c. electric field (E).

1. Room temperature results

Figure 9 shows some chosen $P(E)$ curves obtained at room temperature for different amplitudes of the applied ac electric field. Open curves are an evidence for the existence of a reversible electric polarization, though their shape is uncommon, as the saturation line crosses the horizontal axis instead the vertical one. We have explored this feature in detail by looking at the direction the $P = P(E)$ curve is being drawn. It is ascertained from our data that the clockwise direction is in fact the right one as shown by the arrow in the Figure 9. This outcome is also corroborated by our earlier studies carried out in $KTaO_{3-\delta}$ films deposited on the same substrate by pulsed laser ablation. Moreover, the clockwise direction is kept despite of changes in the upper electrode type (gold or aluminum), reference capacitor magnitude, and electric field frequency (up to 400 Hz).[41] The question now is to find out what are the mechanisms underneath this behavior. Our interpretation assumes the existence of an electric polarization opposite to the applied field, which stems from internal fields originated from the inclusion of oxygen vacancies in the films. The linear part of the $P(E)$ curves is kept for electric field maximum amplitude up to 400 kV/cm. where the film behaves as a linear dielectric.

2. Temperature dependent results

Figure 10 shows some $P(E)$ curves for some fixed temperatures. It can be observed that by increasing temperature, $P(E)$ curves become non-symmetric and the open part continuously shrinks until close to 367 °C, above which $P = P(E)$ curves become linear. At this temperature, the polarized state changes into a non-polarized equilibrium one. Figure 11 shows the temperature dependence of the electric polarization, $P_{E\ 0}(T)$, measured at zero electric external field. From low temperatures up to close to 220 °C, $P_{E\ 0}(T)$ does not change with temperature, whereas thereafter starts to decrease towards 367 °C. It is worth noting that above the temperature where the polarization starts to decrease open cycles become asymmetric. This asymmetry signals the emergence of internal electric fields, associated with significant charge defect rearrangements. The inset of Figure 11 shows the temperature dependence of thermally stimulated depolarization current, $I(T)$. Its maximum also occurs close to 367 °C in agreement with aforementioned results. Furthermore, the broad shape of $I(T)$ still confirms the existence of charge defects in the film.

The $KTaO_{3-\delta}$ films annealed in oxygen atmosphere drastically drops the number of oxygen vacancies and thus do not show any polarized state.

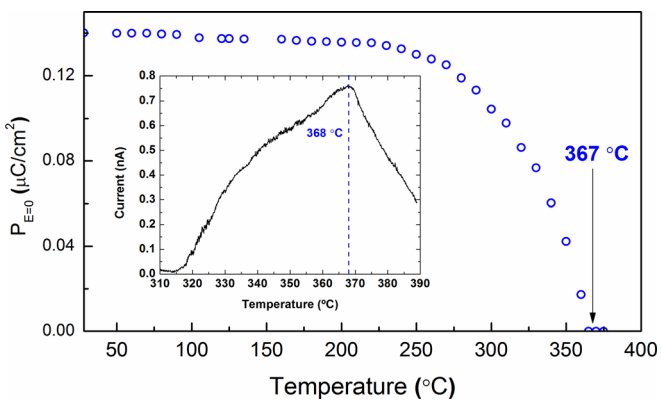

FIG. 11. Electric polarization as a function of the temperature for the $KTaO_{3-\delta}$ thin film. Inset shows temperature dependence of thermally stimulated depolarization current.

IV. CONCLUSIONS

Oxygen deficient potassium tantalate thin films with a thickness around 230 nm were grown by RF magnetron sputtering on $Si/SiO_2/Ti/Pt$ substrates. Room temperature X-rays diffraction analysis provided evidence for the existence of a compressive strain of 2.3% due to the incorporation of oxygen vacancies in the $KTaO_3$ system during deposition. Leakage current studies revealed that carriers follow the Poole-Frenkel formalism showing the presence of charge defects in the film. The existence of a polarized state below ~367 °C was ascertained from dielectric, polarization, and thermally stimulated depolarization current measurements. A Cole-Cole dipolar relaxation was evidenced associated with the reorientation of oxygen vacancies induced dipoles. The $KTaO_{3-\delta}$ films annealed in an oxygen atmosphere at a constant fixed temperature above 367 °C, do not show any polarized state, which is apparently suppressed by drastic oxygen vacancies reduction during the annealing process.

ACKNOWLEDGMENTS

This work was supported by Portuguese Foundation for Science and Technology FCT (PTDC/CTM/64805/2006). A. Tkach also acknowledges FCT for financial support (SFRH/BPD/34607/2007).

[1]V. V. Lemanov, A. V. Sotnikov, E. P. Smirnova, M. Weihnacht, and R. Kunze, Solid State Commun. **110**, 611 (1999).
[2]A. Chen, A. S. Bhalla, and L. E. Cross, Phys. Rev. B **64**, 184104 (2001).
[3]C. H. Perry and T. F. McNelley, Phys. Rev. **154**, 456 (1967).
[4]A. Pashkin, V. Zelezny, and J. Petzelt, J. Phys.: Condens. Matter **17**, L265 (2005).
[5]Y. Ichikawa, M. Nagai, and K. Tanaka, Phys. Rev. B **71**, 092106 (2005).
[6]G. A. Samara, J. Phys.: Condens. Matter **15**, R367 (2003).
[7]J. H. Haeni, P. Irvin, W. Chang, R. Uecker, P. Reiche, Y. L. Li, S. Choudhury, W. Tian, M. E. Hawley, B. Craigo, A. K. Tagantsev, X. Q. Pan, S. K. Streiffer, L. Q. Chen, S. W. Kirchoefer, J. Levy, and D. G. Schlom, Nature (London) **430**, 758 (2004).
[8]D. J. Singh, Phys. Rev. B **53**, 176 (1996).
[9]A. K. Tagantsev, V. O. Sherman, K. F. Astafiev, J. Venkatesh, and N. Setter, J. Electroceram. **11**, 5 (2003).
[10]R. G. Geyer, B. Riddle, J. Krupka, and L. A. Boatner, J. Appl. Phys. **97**, 104111 (2005).
[11]N. A. Pertsev, A. G. Zembilgotov, and A. K. Tagantsev, Phys. Rev. Lett. **80**, 1988 (1998).
[12]N. A. Pertsev, A. K. Tagantsev, and N. Setter, Phys. Rev. B **61**, R825 (2000).
[13]O. Diéguez, S. Tinte, A. Antons, C. Bungaro, J. B. Neaton, K. M. Rabe, and D. Vanderbilt, Phys. Rev. B **69**, 212101 (2004).
[14]O. Diéguez, K. M. Rabe, and D. Vanderbilt, Phys. Rev. B **72**, 144101 (2005).
[15]M. Tyunina, J. Narkilathi, M. Plekh, R. Oja, R. M. Nieminen, A. Dejneka, and V. Trepakov, Phys. Rev. Lett. **104**, 227601 (2010).
[16]V. Skoromets, S. Glinsek, V. Bovtun, M. Kempa, J. Petzelt, S. Kamba, B. Malic, M. Kosec, and P. Kuzel, Appl. Phys. Lett. **99**, 052908 (2011).
[17]V. Železný, J. Buršík, and P. Vaněk, J. Eur. Ceram. Soc. **25**, 2155 (2005).
[18]J. N. Eckstein, Nat. Mater. **6**, 473 (2007).
[19]M. Itoh, R. Wang, Y. Inaguma, T. Yamaguchi, Y. J. Shan, and T. Nakamura, Phys. Rev. Lett. **82**, 3540 (1999).
[20]M. D. Glinchuk, R. O. Kuzian, V. V. Laguta. and I. P. Bykov, *Defects and Surface Induced Effects in Advanced Perovskites* (Springer, Netherlands, 2000), Vol. 77, p. 367.
[21]I. M. Smolyaninov, J. Phys.: Condens. Matter **10**, 10333 (1998).
[22]A. Tkach, P. M. Vilarinho, A. Kholkin, I. M. Reaney, J. Pokorny, and J. Petzelt, Chem. Mater. **19**, 6471 (2007).
[23]S. Jandl, P. Grenier, and L. A. Boatner, Ferroelectrics **107**, 73 (1990).
[24]S. Jandl, M. Banville, P. Dufour, and S. Coulombe, Phys. Rev. B **43**, 7555 (1991).
[25]C. H. Park and D. J. Chadi, Phys. Rev. B **57**, R13961 (1998).
[26]C. C. Wang, C. M. Lei, G. J. Wang, X. H. Sun, T. Li, S. G. Huang, H. Wang, and Y. D. Li, J. Appl. Phys. **113**, 094103 (2013).
[27]R. Chaves, H. Amaral, and S. Ziolkiewicz, J. Physique **41**, 259 (1980).
[28]C. B. Sawyer and C. H. Tower, Phys. Rev. **35**, 269 (1930).
[29]ICDD (International Center for Driffraction Data), $KTaO_3$, Powder Diffraction File No. 04 007 4829 (PDF 4+ Database).
[30]J. Kim, W. Chang, S. B. Qadri, J. M. Pond, S. W. Kirchoefer, D. B. Chrisey, and J. S. Horwitz, Appl. Phys. Lett. **76**, 1185 (2000).
[31]A. Podpirka, M. W. Cole, and S. Ramanathan, Appl. Phys. Lett. **92**, 212906 (2008).
[32]J. Robertson and C. W. Chen, Appl. Phys. Lett. **74**, 1168 (1999).
[33]C. Fu, F. Pan, and W. Cai, Integr. Ferroeletrics **91**, 112 (2007).
[34]J. F. Scott, J. Phys.: Condens. Matter **18**, R361 (2006).
[35]R. C. Miller and W. G. Spitzer, Phys. Rev. **129**, 94 (1963).
[36]M. Fukui, H. Orihara, A. Suziki, Y. Ishibashi, Y. Yamada, N. Yamamoto, K. Mori, K. Nakamura, and Y. Suzuki, Jpn. J. Appl. Phys. **29**, 329 (1990).
[37]K. S. Cole and R. H. Cole, J. Chem. Phys. **9**, 341 (1941).
[38]N. A. Pertsev and A. Y. Emelyanov, Phys. Rev. B **65**, 174115 (2002).
[39]L. Pintilie, I. Vrejoiu, D. Hesse, G. LeRhun, and M. Alexe, Phys. Rev. B **75**, 224113 (2007).
[40]F. Xu, S. Trolier McKinstry, W. Ren, B. Xu, Z. L. Xie, and K. J. Hemker, J. Appl. Phys. **89**, 1336 (2001).
[41]A. Loidl, S. Krohns, J. Hemberger, and P. Lunkenheimer, J. Phys.: Condens. Matter **20**, 191001 (2008).